

Development of dislocation density-reliant physical models to describe the creep and flow stress response of high-temperature materials



**Thesis submitted in partial fulfillment for the
Award of Degree**

Doctor of Philosophy

By

Nilesh Kumar

**DEPARTMENT OF METALLURGICAL ENGINEERING
INDIAN INSTITUTE OF TECHNOLOGY
(BANARAS HINDU UNIVERSITY)
VARANASI - 221005
INDIA**

Roll No. 19141005

Year 2024

Dedicated

To

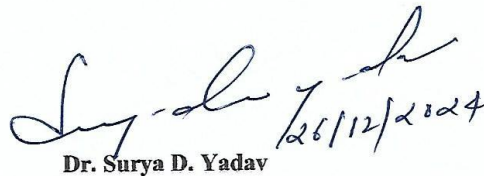
*My Beloved Parents, Elder Brother,
Elder Sister & My Future Better Half*



CERTIFICATE

It is certified that the work contained in the thesis titled “**Development of dislocation density reliant physical models to describe the creep and flow stress response of high temperature materials**” by “**Nilesh Kumar**” has been carried out under my supervision and this work has not been submitted elsewhere for a degree.

It is further certified that the student has fulfilled all the requirements of Comprehensive, Candidacy and SOTA for the award of Ph.D. degree.


26/12/2024

Dr. Surya D. Yadav

(Supervisor)

Assistant Professor

Department of Metallurgical Engineering

Indian Institute of Technology (BHU), Varanasi

Varanasi - 221005, Uttar Pradesh, India

DECLARATION BY THE CANDIDATE

I, **Nilesh Kumar**, certify that the work embodied in this Ph.D. thesis is my own bonafide work carried out by me under the supervision of **Dr. Surya D. Yadav** for a period from **July 2019 to December 2024** at the “**Department of Metallurgical Engineering**”, Indian Institute of Technology (BHU), Varanasi, India. The matter embodied in this Ph.D. thesis has not been submitted for the award of any other degree/diploma. I declare that I have faithfully acknowledged and given credits to the researchers wherever related works has been cited in this thesis. I further declare that I have not copied any other's work, paragraphs, text, data, results, *etc.*, reported in journals, books, magazines, reports dissertations, thesis, *etc.*, or available at websites and have not included them in this thesis and have not cited as my own work.

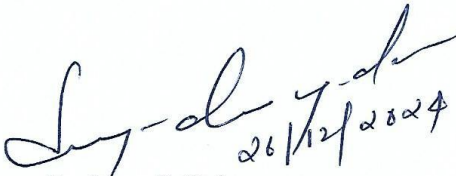
Date: 26/12/2024

Place: Varanasi

Nilesh Kumar
(Nilesh Kumar)

CERTIFICATE BY THE SUPERVISOR

This is to certify that the above statement made by the candidate is correct to the best of our knowledge.



26/12/2024

Dr. Surya D. Yadav

(Supervisor)

Assistant Professor

Department of Metallurgical Engineering

Indian Institute of Technology (BHU), Varanasi

Varanasi - 221005, Uttar Pradesh, India



ForWARDED by:

(Prof. Sunil Mohan)

Head of Department

Department of Metallurgical Engineering

Indian Institute of Technology

(Banaras Hindu University)

Varanasi - 221005, India

COPYRIGHT TRANSFER CERTIFICATE

Title of the Thesis: "Development of dislocation density reliant physical models to describe the creep and flow stress response of high temperature materials".

Candidate's Name: Nilesh Kumar

Copyright Transfer

The undersigned hereby assigns to the Indian Institute of Technology (Banaras Hindu University), Varanasi all rights under copyright that may exist in and for the above thesis submitted for the award of the *Doctor of Philosophy*.

Date: 26/12/2024

Place: Varanasi

Nilesh Kumar
(NILESH KUMAR)

Note: However, the author may reproduce or authorize others to reproduce materials extracted verbatim from the thesis or derivative of the thesis for author's personal use provided that the source and the Institute's copyright notice are indicated.

ACKNOWLEDGEMENT

Before I begin, I want to express my gratitude to the Almighty for helping me over the years I studied and for providing me with the strength I needed to go through the difficult times. I also offer my thanks to the Almighty for granting me the chance to attend the Indian Institute of Technology (BHU), Varanasi, India which was established by the great visionary Mahamana Pandit Madan Mohan Malviya Ji.

I was very fortunate to begin my research work under the esteemed supervision of Dr. Surya D. Yadav. I got support from you in every aspects of pursuing my PhD. Whenever me or student need either technical or non-technical assistance, you are available to resolve the problem. Thanks sir, keeping outside the glass ceiling barriers to continue the research work smoothly. Thanks, for the abroad collaboration to enhance my knowledge and the lab group members too.

I would like to express my gratitude to my advisors as well as the other members of my RPEC, Dr. Ashok Kumar Mondal and Dr. Sanjay Singh (SMST), for their support and enlightening remarks. My deepest gratitude goes out to Prof. Sunil Mohan, Head of the Department of Metallurgical Engineering at IIT (BHU), Varanasi and Prof. N.K. Mukhopadhyay, Former Head of the Department of Metallurgical Engineering at IIT (BHU); for their insightful feedback, helpful suggestions, and essential assistance provided in carrying out my research. For her unwavering support throughout the years, I would like to thank Prof. Cecillia Poletti (Institute of Material Science, Joining and Forming, TU Graz, 8010 Graz, Austria; Christian Doppler for Design of High-Performance Alloys by Thermomechanical Processing). I am grateful to DST India and OEAD Austria for their financial support. Her prompt advice and edits have always been helpful to me. Additionally, I would want to express my gratitude to Dr. Joysurya Basu

for introducing and teaching me how to use SEM on my own. Through his mentoring, I've been able to acquire useful SEM concepts.

I would like to extend my gratitude to Dr. Ashish Kumar Mishra from the School of Material Science and Technology, IIT (BHU) department, for inspiring me to pursue my career in the field of research.

I express my sincere thanks to the all faculty members of the department for their valuable suggestions. I express my gratitude to my friends, Utkarsh Pandey, Shreshtha Ranjan, Ricardo Henrique Buzolin, Esmacil Shahryari, Yogendra Chouksey and Kashyap Pradeep. My profound gratitude to all of the department's non-teaching staff members, including Mr. J P Patel, Mr. Arun Prakash, Mr. Kamala Prasad, Mr. Chotey Lal, Mr. Ramji, and Mr. Anjani.

With heartfelt gratitude to my brother, sister, and parents, whose unwavering support and love have made this journey possible. There are no words to describe the sacrifices they have made on my behalf. Their assistance, moral support, and spiritual guidance have enabled me to get through challenging times.

Nilesh Kumar
Nilesh Kumar

Contents

| | |
|---------------------------|----------------|
| List of Figures..... | (v)-(ix) |
| List of Tables..... | (x) |
| Nomenclature..... | (xi)-(xvi) |
| List of Publications..... | (xvii) |
| List of Conferences..... | (xvii)-(xviii) |
| PREFACE..... | (xix)-(xxviii) |

Chapter 01. Introduction and literature review1

| | |
|---|----|
| 1.1. High temperature structural materials and micromechanical deformation modelling..... | 1 |
| 1.2. Empirical based flow stress models..... | 2 |
| 1.2.1. Johnson–Cook Model, 1983..... | 2 |
| 1.2.2. Zerilli–Armstrong Model, 1987..... | 3 |
| 1.2.3. Y.C Lin and X.M. Chen Model, 2010..... | 3 |
| 1.3. Physics Based Flow Stress Model..... | 4 |
| 1.3.1. Y. Bergström Model, 1970..... | 4 |
| 1.3.2. F. Barlat et al. Model, 2002..... | 5 |
| 1.3.3. Y.C. Lin and D.X. Wen Model, 2014, 2016..... | 6 |
| 1.3.4. X. Tang et al. Model, 2016..... | 7 |
| 1.3.5. L. E. Lindgren et al. Model, 2017..... | 8 |
| 1.3.6. R. Wang et al. Model, 2018..... | 10 |
| 1.3.7. H. Li et al. Model, 2019..... | 10 |
| 1.3.8. Surya D. Yadav et al. Model, 2019..... | 12 |
| 1.4. Empirical based creep models..... | 13 |
| 1.4.1. M. McLean and B. F. Dyson Model, 2000..... | 13 |
| 1.4.2. Y. Yin and R.Faulkner Model, 2006..... | 13 |
| 1.4.3. N. Bonora and L. Esposito Model, 2008..... | 14 |
| 1.4.4. B. Xiao et al. Model, 2019..... | 14 |
| 1.5. Physics-based creep models..... | 15 |
| 1.5.1. N.M. Ghoniem et al. Model, 1990..... | 15 |
| 1.5.2. H. Magnusson et al. Model, 2007..... | 15 |
| 1.5.3. H. Semba et al. Model, 2008..... | 17 |
| 1.5.4. B.F. Dyson Model, 2008..... | 17 |

| | | |
|--------|--|----|
| 1.5.5. | F. Krumphal et al. Model, 2009..... | 18 |
| 1.5.6. | M. Basirat et al. Model, 2012 | 18 |
| 1.5.6. | Y.K Kim et al. Model, 2016 | 19 |
| 1.5.7. | Surya D. Yadav et al. Model, 2016, 2018..... | 19 |
| 1.5.8. | C.Ó Murchú et al. Model, 2017 | 21 |
| 1.5.9. | S. Wu et al. Model, 2022 | 21 |
| 1.6. | Problem definitions..... | 22 |

Chapter 02. A meso-scale model to predict flow stress and microstructure

during hot deformation of IN718WP25

| | | |
|--------|---|----|
| 2.1. | Introduction | 25 |
| 2.2. | Materials and Methods | 29 |
| 2.3. | Model Formulation..... | 31 |
| 2.3.1. | Constitutive equations..... | 32 |
| 2.3.2. | Microstructural rate equations..... | 35 |
| 2.3.3. | Mean free path of glide | 38 |
| 2.3.4. | Discontinuous dynamic recrystallization (DDRX)..... | 39 |
| 2.4. | Solution for constitutive equations and optimization of parameters..... | 43 |
| 2.5. | Results and discussion..... | 47 |
| 2.5.1. | Flow curves..... | 47 |
| 2.5.2. | DDRX fraction and average grain size | 50 |
| 2.5.3. | Evolutions of dislocation density..... | 55 |
| 2.5.4. | Glide velocities and climb velocities..... | 58 |
| 2.6. | Summary and Conclusions..... | 60 |

Chapter 03. Microstructure based flow stress modelling of superalloy 71863

| | | |
|------|-----------------------------|----|
| 3.1. | Introduction | 63 |
| 3.2. | Methodology | 64 |
| 3.3. | Model Formulation..... | 65 |
| 3.4. | Results and discussion..... | 67 |
| 3.5. | Conclusions | 71 |

Chapter 04. An improved dislocation density reliant model to address the

creep deformation of reduced activation ferritic martensitic steel.72

| | |
|---|-----|
| 4.1. Introduction | 72 |
| 4.2. Materials and methods | 77 |
| 4.3. Model formulation..... | 78 |
| 4.3.1. Representation of the microstructure | 78 |
| 4.3.2. Framework of microstructure based hybrid model..... | 79 |
| 4.4. Results and discussion..... | 86 |
| 4.4.1. Creep Strain | 86 |
| 4.4.2. Substructure evolution led by creep..... | 87 |
| 4.4.3. Creep led changes in internal stress, effective stress, climb stress, glide velocity, climb velocity and dipole capture spacing | 93 |
| 4.4.4. Evolution of subgrain boundary mobility, boundary dislocation spacing and boundary pressure..... | 97 |
| 4.4.5. Occurrence of damage due to precipitate coarsening and cavitation..... | 99 |
| 4.4.6. Influence of applied stress on model parameters..... | 101 |
| 4.5. Significance and effectiveness of the model | 104 |
| 4.6. Summary and conclusions..... | 105 |

Chapter 05. A dislocation density reliant mean-field model to describe the creep response and microstructure evolution of superalloy IN-718 ..109

| | |
|---|-----|
| 5.1. Introduction | 109 |
| 5.2. Experimental | 112 |
| 5.2.1. Material and uniaxial tensile creep testing..... | 112 |
| 5.2.2. Microstructure characterization | 112 |
| 5.3. Model formulation..... | 113 |
| 5.3.1. Microstructure conceptualization..... | 113 |
| 5.3.2. Precipitates and other obstacles | 115 |
| 5.3.3. Constitutive equations: internal and effective stresses and creep strain | 117 |
| 5.3.4. Glide velocity, climb velocity and climb stress and the influence of SFE | 118 |
| 5.4. Model set up..... | 119 |
| 5.5. Results and Discussion..... | 121 |
| 5.5.1. Creep strain | 121 |

| | | |
|--|--|------------|
| 5.5.2. | Substructure evolutions..... | 122 |
| 5.5.3. | Evolution of mean free path..... | 125 |
| 5.5.4. | Evolution of internal stress, effective stress, climb stress and glide velocity..... | 126 |
| 5.5.5. | Microstructure..... | 130 |
| 5.6. | Conclusions | 133 |
| Chapter 06. Microstructure-based creep strain modeling of steel 316LN at 140-275 MPa / 600-650 °C... .. | | 136 |
| 6.1. | Introduction | 136 |
| 6.2. | Material and input parameters..... | 140 |
| 6.3. | Creep model for steel 316 LN..... | 141 |
| 6.3.1. | Microstructure consideration and its evolution..... | 141 |
| 6.3.2. | Internal stress and effective stress..... | 143 |
| 6.3.3. | Dislocation velocity and dislocation mobility | 144 |
| 6.3.4. | Damage | 145 |
| 6.3.5. | Creep strain | 147 |
| 6.4. | Results and discussion..... | 147 |
| 6.4.1. | Creep curves..... | 147 |
| 6.4.2. | Microstructure evolution..... | 148 |
| 6.4.3. | Internal stress, effective stress, dislocation velocity, and dislocation mobility | 152 |
| 6.4.4. | Damage evolution | 155 |
| 6.4.5. | Applicability and usefulness of this model..... | 159 |
| 6.5. | Summary and Conclusions..... | 160 |
| Chapter 07. Summary and conclusions..... | | 163 |
| 7.1. | Summary and Conclusions..... | 163 |
| 7.2. | Outlook..... | 167 |
| References..... | | 168 |

List of Figures

| | |
|---|----|
| Figure 2.1. BSE image showing the microstructure of the as-received IN718WP..... | 31 |
| Figure 2.2. Schematic of the assumed microstructure of IN718WP superalloy..... | 31 |
| Figure 2.3. Schematic diagram depicting the different possibilities of dislocation interactions that enable estimating the mean free path..... | 39 |
| Figure 2.4. Illustration of the microstructure in IN718WP; (a) as-received condition, (b) before reaching the ρ_c for DDRX, (c) reaching ρ_c (d) after reaching ρ_c during deformation... | 42 |
| Figure 2.5. Schematic illustration of the mean-field model proposed in this work..... | 46 |
| Figure 2.6. Experimental and simulated flow stress curves of IN718WP at different strain rates (0.001 s ⁻¹ - 10 s ⁻¹) and temperature (a) 900 °C, (b) 925 °C, (c) 950 °C, (d) 975 °C, (e) 1000 °C and (f) 1025 °C..... | 48 |
| Figure 2.7. Experimental and simulated flow stress curve of IN718WP at 900 °C - 1025 °C / 1 s ⁻¹ | 49 |
| Figure 2.8. As received IN718WP superalloy (a) IPF Map and (b) KAM Map..... | 50 |
| Figure 2.9. Variation of predicted average grain size and recrystallization fraction at (a) 925 °C- 1025 °C / 0.1 s ⁻¹ and (b) 0.01 s ⁻¹ - 10 s ⁻¹ / 1000 °C..... | 51 |
| Figure 2.10. Hot compressed IN718WP superalloy: IPF map (a and d); KAM map (b and e); GOS map (c and f) for , 900 °C/ 0.001 s ⁻¹ , 1000 °C / 0.1 s ⁻¹ and 1000 °C / 0.01 s ⁻¹ , respectively..... | 52 |
| Figure 2.11. (ODF) Map for the section $\phi=45^\circ$ and 65° at 0.8 strain (a) 1000 °C / 0.1 s ⁻¹ and (c) 1000 °C / 0.01 s ⁻¹ | 53 |
| Figure 2.12. Comparison of simulated and experimentally measured recrystallization fraction (from GOS map) at the end of deformation for 1000 °C / 0.01 s ⁻¹ and 1000 °C / 0.1 s ⁻¹ | 55 |
| Figure 2.13. Evolutions of immobile and mobile dislocation density for IN718WP superalloy (a and c) 925 °C - 1025 °C / 0.1 s ⁻¹ and (b and d) 1000 °C / 0.01 s ⁻¹ - 10 s ⁻¹ | 56 |
| Figure 2.14. ρ_b calculated from EBSD data and ρ_i predicted from model (a) As received, 1000 °C / 0.01 s ⁻¹ and 1000 °C / 0.1 s ⁻¹ | 57 |
| Figure 2.15. (a, c) Temperature effect on the v_{gl} and v_{cl} at 0.1 s ⁻¹ , (b, d) Strain rate effect on the v_{gl} and v_{cl} at 1000 °C..... | 59 |

Figure 3.1. σ_{flow} vs. true plastic strain curves of IN 718 alloy with considering the modified Hall-Petch equation incorporating the annealing twin boundaries at 873 K (a) $1.0 \times 10^{-2.0} s^{-1}$, (b) $1.0 \times 10^{-1.0} s^{-1}$ and at 1073 K (c) $1.0 \times 10^{-2.0} s^{-1}$, (d) $1.0 \times 10^{-1.0} s^{-1}$ 68

Figure 3.2. Variation of ρ and s of IN 718 alloy is plotted with ongoing strain at 873 K (a) $1.0 \times 10^{-2.0} s^{-1}$, (b) $1.0 \times 10^{-1.0} s^{-1}$ and at 1073 K (c) $1.0 \times 10^{-2.0} s^{-1}$, (d) $1.0 \times 10^{-1.0} s^{-1}$ 69

Figure 3.3. σ_{flow} vs. true plastic strain curves of IN 718 alloy using traditional Hall-Petch equation without considering the effect of annealing twins at 873 K (a) $1.0 \times 10^{-2.0} s^{-1}$, (b) $1.0 \times 10^{-1.0} s^{-1}$ and at 1073 K (c) $1.0 \times 10^{-2.0} s^{-1}$, (d) $1.0 \times 10^{-1.0} s^{-1}$ 70

Figure 4.1. Schematic diagram of the representative microstructure of as-received tempered RAFM steel 78

Figure 4.2. Different microstructural interactions inside a subgrain. (i) Signifies the production of mobile dislocations, (ii) Signifies glide/dynamic recovery of mobile and dipole dislocations, (ii) Signifies the Climb recovery of mobile and dipole dislocations, (ii) Signifies the Climb recovery of mobile and dipole dislocations, (iv) Formation of dipole dislocations, (v) Conversion of the dipole dislocation in to boundary dislocations. (vi) ΔR_{sub} signifies the subgrain growth, (vii) Coarsening of carbide and carbonitride precipitate and (viii) Represents the cavitation phenomena 79

Figure 4.3. Simulated vs. experimental creep curves of RAFM steel at (a) 280 MPa / 500 °C (b) 140 MPa / 600 °C, (c) 200 MPa / 550 °C, (d) 120 MPa / 600°C. Experimental creep curves are obtained from literature. 86

Figure 4.4. Output parameters of model vs. time curves for 500 °C / 280 MPa (a) Mobile dislocation density, (b) Dipole dislocation density, (c) Boundary dislocation density, (d) Subgrain radius, (e) Glide velocity, (f) Climb velocity, (g) Internal stress, (h) Effective stress, (i) Boundary pressure, (j) Radius of MX precipitate, (k) Softening of MX precipitate, (l) Radius of M23C6 precipitate (m) Softening of M23C6 precipitate, (n) Cavitation softening, (o) Boundary dislocation spacing, (p) Subgrain boundary mobility, (q) Dipole capture spacing and (r) Climb stress 88

Figure 4.5. Output parameters of model vs. time curves for 550 °C / 200 MPa (a) Mobile

dislocation density, (b) Dipole dislocation density, (c) Boundary dislocation density, (d) Subgrain radius, (e) Glide velocity, (f) Climb velocity, (g) Internal stress, (h) Effective stress, (i) Boundary pressure, (j) Radius of MX precipitate, (k) Softening of MX precipitate, (l) Radius of M23C6 precipitate (m) Softening of M23C6 precipitate, (n) Cavitation softening, (o) Boundary dislocation spacing, (p) Subgrain boundary mobility, (q) Dipole capture spacing and (r) Climb stress..... 89

Figure 4.6.Schematic diagram of the proposed substructure evolution during creep of RAFM steel 93

Figure 4.7.Influence of stress 120 MPa 140 MPa on the modeled parameter at 600 °C (a) Mobile dislocation density, (b) Dipole dislocation density, (c) Boundary dislocation density, (d) Subgrain radius, (e) Glide velocity, (f) Climb velocity, (g) Internal stress, (h) Effective stress, (i) Boundary pressure, (j) Radius of MX precipitate, (k) Softening of MX precipitate, (l) Radius of M23C6 precipitate (m) Softening of M23C6 precipitate, (n) Cavitation softening, (o) Boundary dislocation spacing, (p) Subgrain boundary mobility, (q) Dipole capture spacing and (r) Climb stress..... 102

Figure 5.1.Representative microstructure of as received IN-718 superalloy considered in the model..... 114

Figure 5.2.Schematic diagram illustrating the different obstacles a mobile dislocation may encounter during the travel 116

Figure 5.3.Simulated vs. experimental creep curves of IN-718 superalloy at (a) 593 °C / 552 MPa, 662 MPa, and 827 MPa; (b) 620 °C / 552 MPa, 662 MPa, and 827 MPa; (c) 650 °C / 552 MPa and 662 MPa 121

Figure 5.4.Predicted ρ_m vs. time of IN 718 superalloy at (a) 593 °C / 552, 662 and 827 MPa, (b) 620 °C / 552, 662 and 827 MPa, (c) 650 °C / 552 and 662 MPa 123

Figure 5.5.The evolution ρ_i of IN-718 superalloy at (a) 593 °C / 552, 662, and 827 MPa (b) 620 °C / 552, 662, and 827 MPa (c) 650 °C / 552 and 662 MPa..... 124

Figure 5.6.The evolution of λ_{mean} for IN-718 superalloy at (a) 593 °C / 552 MPa, 662 MPa and 827 MPa; (b) 620 °C / 552 MPa, 662 MPa and 827 MPa; (c) 650 °C / 552 MPa, and 662 MPa..... 125

Figure 5.7.The evolution of h_m , s , L_p , γ' , L_p , γ'' and λ_{mean} for IN-718 superalloy at 593 °C / 552

| | |
|--|-----|
| MPa..... | 126 |
| Figure 5.8. Predicted σ_{int} , σ_{effe} and σ_{cl} vs. time curves of IN-718 superalloy at 620 °C / 552 MPa | 127 |
| Figure 5.9. Predicted v_{gl} vs. time of a IN-718 superalloy at (a) 593 °C / 552-827 MPa, (b) 620 °C / 552-827 MPa, (c) 650 °C / 552-662 MPa | 129 |
| Figure 5.10. As received IN-718 superalloy (a) IPF Map and (b) KAM Map | 130 |
| Figure 5.11. Crept IN-718 superalloy: IPF map and KAM map at 593 °C / 662 (a and b) and at 593 °C / 827 MPa (c and d)..... | 131 |
| Figure 5.12. ρ_b from EBSD data and ρ_i from the model prediction for 593 °C / 662 and 593 °C / 827 MPa. ρ_b from EBSD data for as received..... | 132 |
| Figure 6.1. TEM micrograph of as received 316 LN stainless steel sample | 140 |
| Figure 6.2. Experimental and modelled creep curves of steel 316 LN; (a) Black solid line and circle: 175 MPa, blue triangle and solid line: 225 MPa, green square and solid line: 250MPa Magenta pentagon and solid line: 275 MPa at 600 °C and (b) Black solid line and circle: 140 MPa, Blue triangle and solid line: 175 MPa, Green square and solid line: 200MPa, Magenta pentagon and solid line: 225 MPa at 650 °C. | 148 |
| Figure 6.3. Influence of σ_{appl} on dislocation density; (a) Mobile: black line / 225 MPa, Green line / 250 MPa; Forest: red line / 225 MPa, blue line / 250 MPa at 600 °C, (b) Mobile : black line / 140 MPa, Green line / 175 MPa; Forest: red line / 140 MPa, blue line / 175 MPa at 650 °C and mean free path: (c) black line / 225 MPa, red line / 250 MPa at 600 °C, (d) black line / 140 MPa, red line / 175 MPa and at 650 °C. “ * ” symbol in Figure. 6.3b represents experimental value of forest dislocation density. | 150 |
| Figure 6.4. TEM micrograph of 316 LN steel (a) 650 °C / 140 MPa | 151 |
| Figure 6.5. Influence of σ_{appl} on radius of precipitates, (a) $M_{23}C_6$ -type: black line / 225 MPa, red line / 250 MPa at 600 °C, (b) $M_{23}C_6$ -type: black line / 140 MPa, red line / 175 MPa at 650 °C, (c) MX-type: black line / 225 MPa, red line / 250 MPa at 600 °C, (d) MX- type: black line / 140 MPa, red line / 175 MPa at 650 °C..... | 152 |
| Figure 6.6. Influence of σ_{appl} on internal stress; (a) black line / 225 MPa, red line / 250 MPa at 600 °C, (b) black line / 140 MPa, red line / 175 MPa at 650 °C and effective stress; (c) black line / 225 MPa, red line / 250 MPa, at 600 °C, (d) black line / 140 MPa, red | |

| | |
|---|-----|
| line / 175 MPa at 650 °C..... | 153 |
| Figure 6.7. Influence of σ_{appl} on dislocation velocity; (a) black line / 225 MPa, red line / 250 MPa at 600 °C, (b) black line / 140 MPa, red line / 175 MPa at 650 °C and dislocation mobility; (c) black line / 225 MPa, red line / 250 MPa, at 600 °C, (d) black line / 140 MPa, red line / 175 MPa at 650 °C. | 155 |
| Figure 6.8. Influence of σ_{appl} on precipitate coarsening damage (a) $M_{23}C_6$ -type: black line / 225 MPa, red line / 250 at 600 °C, (b) $M_{23}C_6$ -type: black line / 140 MPa, red line / 175 at 650 °C, (c) MX-type: black line / 225 MPa, red line / 250 at 600 °C, (d) MX-type: black line / 140 MPa, red line / 175 at 650 °C; (e) Cavitation: black line / 225 MPa, red line / 250 at 600 °C, (d) Cavitation: black line / 140 MPa, red line / 175 at 650 °C | 157 |
| Figure 6.9. Optical micrograph of crept samples at 650 °C (a) 175 MPa, (b) 200 MPa..... | 158 |

List of Tables

| | |
|---|-----|
| Table 2.1. Chemical composition of IN718WP alloy..... | 30 |
| Table 2.2. Microstructure-based parameters calibrated as input for this work..... | 44 |
| Table 2.3. Material constants used in the model..... | 46 |
| Table 2.4. Optimized parameters used in the model..... | 47 |
| Table 2.5. Dislocation density predicted in the literature at 0.8 strain..... | 57 |
| Table 3.1. Strength contributions at the end of simulation for different conditions..... | 69 |
| Table 3.2. Model parameters taken from the literature..... | 71 |
| Table 3.3. Model calibrated parameters..... | 71 |
| Table 4.1. Input parameters for simulation..... | 78 |
| Table 4.2. Creep model and corresponding set of equations..... | 82 |
| Table 4.3. Dislocation densities and subgrain radius at the end of the creep/simulation..... | 91 |
| Table 4.4. Model parameters utilized for the simulation of RAFM Steel..... | 107 |
| Table 4.5. Material Constants utilized for the simulation of RAFM Steel..... | 107 |
| Table 5.1. Details of Inconel®718 in terms of alloying elements..... | 112 |
| Table 5.2. Input parameters for creep model of IN-718 superalloy..... | 119 |
| Table 5.3. Material constants used for IN-718..... | 120 |
| Table 5.4. Calibrated parameters incorporated in the model..... | 120 |
| Table 5.5. Dislocation density reported in the literature for Ni-based superalloys after different creep conditions..... | 125 |
| Table 6.1. Initial input parameters used in the model..... | 141 |
| Table 6.2. Output of model at the end of simulation..... | 151 |
| Table 6.3. Microstructural parameters reported in literature for Fe based alloys..... | 154 |
| Table 6.4. Material constants for 316 LN..... | 162 |
| Table 6.5. Parameters for the creep simulation of 316 LN..... | 162 |

Nomenclature

| | |
|--------------------|--|
| H | internal stress generation |
| $\dot{\epsilon}_0$ | constant |
| D_d | damage due to dislocation accumulation |
| D_s | damage due to solute depletion |
| D_{ppt} | damage due to precipitate coarsening |
| D_N | damage due to nucleation of voids |
| D_{cav} | damage due to cavitation |
| D_{cr} | Damage due to chromium depletion |
| k_B | Boltzmann Constant |
| GBS | grain boundary sliding |
| IDG | intragranular deformation glide |
| IDC | intragranular deformation climb |
| ϵ_{GBS} | minimum creep rates due to GBS |
| ϵ_{IDG} | minimum creep rates due to IDG |
| ϵ_{IDC} | minimum creep rates due to IDC |
| σ | stress |
| σ_{appl} | applied stress |
| D_v | lattice diffusion coefficient |
| $\dot{\lambda}$ | plastic multiplier |
| f_d | damage dissipation potential |
| Y | damage variable |
| Q_1 | activation energies of GBS |
| Q_2 | activation energies of IDG |
| Q_3 | activation energies of IDC |
| R | gas constant |
| p | stress exponents for the mechanisms of GBS |
| n | stress exponents for the mechanisms of IDG |
| m | stress exponents for the mechanisms of IDC |
| T | temperature |
| M | Taylor factor |
| b | Burgers vector |
| γ_{sub} | low-angle subgrain boundary energy |
| r_p | radius of precipitate |
| N_p | Number density of precipitate |
| M_{sub} | mobility of subgrains |
| G | room temperature shear modulus |
| G_T | temperature dependent shear modulus |
| v_{cs} | climb velocity of static dislocation |

| | |
|---------------------|---|
| v_{cm} | climb velocity of mobile dislocation |
| v_{gl} | dislocation glide velocity |
| ρ_m | mobile dislocation density |
| ρ_i | immobile dislocation density |
| ρ_f | forest dislocation density |
| ρ_{free} | free dislocation density |
| ρ_{dip} | dipole dislocation density |
| ρ_N | network dislocation density |
| ρ_s | static dislocation density |
| ρ_b | boundary dislocation density |
| R_{sub} | subgrain radius |
| $R_{sub,inf}$ | limiting subgrain size |
| β | factor controlling the source of dislocations |
| h | dislocation spacing within the walls |
| δ | spontaneous annihilation distance |
| n_v | transfer coefficient of vacancies from the dislocation core to jogs |
| k_c | constant |
| D_L | lattice diffusion coefficient |
| D_s | solute diffusion coefficient |
| D_{gb} | grain boundary diffusion coefficient |
| D_{vp} | pipe diffusion coefficient |
| L_{im} | immobile dislocation spacing |
| M_{cl} | dislocation climb mobility |
| T_L | dislocation line tension |
| n_{slip} | number of slip systems |
| d_{lock} | critical distance for the dislocation lock |
| α | constant |
| Q_c | the activation energy for creep |
| A_N | Constant |
| Q_c | Activation energy for creep |
| $\sigma_{back,tot}$ | total back stress |
| N | creep exponent |
| n_g | number of active slip plane |
| CDM | continuum damage mechanics |
| C_j | dislocation jog density |
| H_w | work hardening coefficient due to dislocation pile |
| τ_g | glide resistance for grain boundary sliding |
| τ_c | climb resistance for grain boundary sliding |
| g | grain size |
| h | dislocation climb distance against precipitates |

| | |
|---------------------|---|
| ϕ_p | volume fraction of hard particle |
| λ_p | interparticle spacing |
| τ_D | effective shear stress |
| C | damage constant |
| Δf | Helmholtz free energy |
| Γ | stacking fault factor |
| φ | volume fraction γ' precipitates |
| $\lambda_{\gamma'}$ | γ' precipitate spacing |
| $\dot{\epsilon}_m$ | Minimum strain rate |
| $\dot{\epsilon}$ | strain rate |
| ϵ | strain |
| σ_{flow} | Flow stress |
| WH | work hardening |
| DRV | dynamic recovery |
| DRX | dynamic recrystallization |
| n | strain rate sensitivity |
| α_1 | material constant |
| f_w | work hardening coefficient |
| g_{avg} | average grain size. |
| f_v | dynamic recovery coefficient |
| f_{drx} | dynamic recrystallization coefficient |
| ρ_{i-cr} | dislocation density in new dynamically recrystallized grain |
| s | Substructure size |
| σ_0 | short range stress |
| T^{*m} | homologous temperature |
| ϵ_{ref} | reference strain rate |
| X_{drx} | recrystallization volume fraction |
| l | lamellar thickness |
| c_0 | material constant |
| M_{gb} | grain boundary mobility |
| S | dynamic globularization |
| λ_{mean} | mean free path |
| K_{Lm} | saturation rate of mobile dislocation |
| λ_{ms} | mean saturation-free path |
| δ | grain boundary thickness |
| D_s | self-diffusion coefficient |
| Q_{gb} | activation energy of grain boundary |
| XRD | X-ray diffraction |
| TEM | Transmission electron microscope |

| | |
|-----------------|---|
| LSFE | Low stacking fault energy |
| HSFE | High stacking fault energy |
| RAFM | Reduced activation ferritic martensitic stainless steel |
| DA | direct aging |
| EBSD | electron backscattered diffraction |
| IPF | inverse pole figure |
| KAM | kernel average misorientation |
| w_i | weight factor for immobile dislocation |
| α | dislocation interaction parameter |
| σ_{int} | internal stress |
| σ_{effe} | effective stress |
| X | Stacking fault energy |
| L_p | Mean spacing of precipita |
| a_l | prefactor for the gliding velocity |
| σ_{cl} | climb stress |
| ϑ | Poisson's ratio |
| M_{sb} | mobility of subgrain boundary |
| γ_{sb} | surface energy of subgrain boundary |
| N_{vi} | number density of i^{th} precipitate |
| D_{vp} | core diffusion coefficient |
| Ω | atomic volume |
| c_{dip} | weight factor for dipole dislocation |
| D_{sd} | solute diffusion coefficient |
| B_{vis} | dislocation mobility |
| C_0 | solute concentration |
| r_2 | outer cut off radius |
| r_1 | inner cut off radius |
| ε_a | relative size misfit between solute and solvent atom |
| c_f | weight factor for forest dislocation |
| v_{cg} | glide climb dislocation velocity |
| M_{cg} | glide climb dislocation mobility |
| k_{di} | Ostwald coarsening constant |
| r_{pi} | radius of i^{th} precipitates |
| M_{sb} | subgrain boundary mobility |
| P_{sb} | boundary pressure |
| M_{sb} | subgrain boundary mobility |
| h_b | boundary dislocation spacing |
| h_m | mobile dislocation spacing |
| DDRX | discontinuous dynamic recrystallization |
| SH | strain hardening |

| | |
|---------------------|---|
| DRV | dynamic recovery |
| DRX | dynamic recrystallization |
| GDRX | geometric dynamic recrystallization |
| CDRX | continuous dynamic recrystallization |
| LAGBs | low-angle grain boundaries |
| HAGBs | high-angle grain boundaries |
| DSA | dynamic strain aging |
| WP | without precipitate/ precipitate free |
| OP-S | oxide polishing suspension |
| GOS | grain orientation spread |
| GNDs | geometrically necessary dislocations |
| σ_{dis} | strength contribution due to dislocations |
| σ_{HP} | strength contribution due to grain size |
| σ_{ss} | strength contribution due to solid solutions |
| σ_{gen} | strength contribution due to interaction among orthogonal dislocations |
| H_{sol} | energy barrier to dislocation motion |
| $\sigma_{ss,0}$ | zero temperature yield stress |
| N_{cell} | number of atoms in the unit cell |
| X_i | mole fraction of the <i>i</i> th alloying element |
| δ_i | size misfit due to <i>i</i> th alloying element |
| η'_i | modulus misfit due to <i>i</i> th alloying element |
| v_0 | attempt frequency |
| ΔG | activation energy needed to overcome the obstacles |
| $\sigma_{SR_{eff}}$ | difference between the total flow stress and athermal stress |
| η | coefficient for transfer of defects into jogs |
| L_{climb} | length associated with elastic interactions between dislocation and defects |
| C_k | dislocation interaction coefficient |
| ρ_c | critical dislocation density for DDRX |
| M_{gb} | mobility of the grain boundary |
| Q_{gb} | activation energy for grain boundary diffusion |
| δ | grain boundary thickness |
| τ | dislocation line energy |
| γ_{gb} | grain boundary energy per unit area |
| θ_m | misorientation angle of HAGBs |
| Q_n | activation energy for DDRX |
| X_{DDRX} | DDRX recrystallization fraction |
| v | velocity of the grain boundary |
| P | pressure on the grain boundary |
| q | shape factor |
| N | number of DDRX nuclei |

| | |
|-----------------|--|
| t | time |
| g_{drx} | dynamic recrystallized grain size |
| F_{drx} | dynamic recrystallization coefficient |
| λ_{dis} | average dislocation distance for climb |
| g_{eff} | effective grain size |
| LR | long-range |
| SR | short-range |
| TBs | twin boundaries |
| ρ_{grwn} | grown dislocation density |

List of Publications

1. **N. Kumar**, A.S. Joseph, P. Mehrotra, Surya D. Yadav, An improved dislocation density reliant model to address the creep deformation of reduced activation ferritic martensitic steel, **Forces in Mechanics** 9 (2022) 100117.
2. **N. Kumar**, Surya D. Yadav, Modelling the creep curves of RAFM steel employing a dislocation density reliant model, **Materials Today: Proceedings** 74 (2023) 910-915.
3. **N. Kumar**, Surya D. Yadav, Creep curve modelling of Austenitic Steel 316LN, IOP Conference Series: **Materials Science and Engineering**, IOP Publishing, 2022, p. 012022.
4. **N. Kumar**, Surya D. Yadav, Microstructure Based Flow Stress Modelling of Superalloy 718, *Solid State Phenomena* 353 (2023) 103-108.
5. **N. Kumar**, R.H.Buzolin, E. Shahryari, K. Pradeep, M. C. Poletti and Surya D. Yadav, A dislocation density reliant mean-field model to describe the creep response and microstructure evolution of superalloy IN-718. **Accepted in Trans. Indian Inst. Met.**
6. **N. Kumar**, F. M.B.Ferraz, R.H.Buzolin, E. Shahryari, M. C. Poletti and Surya D. Yadav, A meso-scale model to predict flow stress and microstructure during hot deformation of precipitate-free IN718WP. **Under review.**
7. **N. Kumar** and Surya D. Yadav Creep curve modelling of Austenitic Steel 316LN. **Under review.**
8. A. S. Joseph, P. Gupta, **N. Kumar**, M. C. Poletti, and Surya D. Yadav. 2022. "An advanced dislocation density-based approach to model the tensile flow behaviour of a 64.7 Ni–31.96 Cu alloy." **Philosophical Magazine** 102 (15):1481-1504.
9. P. Mehrotra, **N. Kumar**, A. George, K. C. Sahoo, V. Ganesan, M. R. Ahmadi, S. Trivedi, and Surya D Yadav. 2022. "An advanced mean field dislocation density reliant physical model to predict the creep deformation of 304HCu austenitic stainless steel." **Materials Today Communications** 32:104128.
10. A. Kumar, **N. Kumar**, M. K. Mahto, Surya D. Yadav, M. Vashista, and M. Z. K. Yusufzai. 2023. "Impression creep behaviour of different zones of pulsed gas tungsten arc welded Ti-6Al-4V alloy." **Materials Today Communications** 36:106722.
11. P. Kashyap, G. Sainath, **N. Kumar**, and Surya D. Yadav. 2023. "On the Deformation Mechanism and Dislocation Density Evolution in A Polycrystalline Nano Copper at 10 K–700 K/108 s– 1–109 s– 1 Employing Molecular Dynamics Simulations."The International Conference on Metallurgical Engineering and Centenary Celebration.

List of Conferences

1. Poster presentation titled “A dislocation creep model to study the creep deformation behavior in the nickel based disk superalloys” at the **16th International Conference on Creep and Fracture of Engineering Materials and Structures held during 28th July –**

2nd August 2024, organized by Department of Materials Engineering, Indian Institute of Science, Bengaluru.

2. Oral presentation titled “On the Deformation Mechanism and Dislocation Density Evolution in A Polycrystalline Nano Copper at $10\text{ K}–700\text{ K}/10^8\text{ s}^{-1}–10^9\text{ s}^{-1}$ Employing Molecular Dynamics Simulations.” **Proceedings of the International Conference on Metallurgical Engineering and Centenary Celebration METCENT-2023, 26-28 October, Varanasi, India.**
3. Oral presentation titled “Microstructure Based Flow Stress Modelling of Superalloy 718” at the International Conference on **PROCESSING & MANUFACTURING OF ADVANCED MATERIALS Processing, Fabrication, Properties, Applications was held from July 2 - 7, 2023 Vienna, Austria.**
4. Oral presentation titled “Creep curve modelling of Austenitic Stainless Steel 316LN” at the **76th annual technical meeting of Indian Institute of Metal held at Hyderabad** during 13-16 Nov 2022.
5. Oral presentation titled “Modelling the creep curves of RAFM steel employing a dislocation density reliant model” at **3rd International Conference on Recent Advances in Mechanical Engineering Research and Development (ICRAMERD-2022)** held on August 11 to 13, 2022 and organized by Department of Mechanical Engineering, ITER, Siksha 'O' Anusandhan (Deemed to be University), Bhubaneswar-751030, Odisha, India.
6. Oral presentation titled titled “Creep curve modelling of Austenitic Steel 316LN” at **2nd International Conference on Materials Science and Engineering (ICMSE-2022) held on June 11-12, 2022** and organized by the Department of Mechanical Engineering, Dr. B R Ambedkar National Institute of Technology, Jalandhar, Punjab, India
7. Oral presentation titled “Creep curve modelling of Reduced activation ferritic-Martensitic(RAFM) steel” in **CF-8 web conference held during August 24-27, 2021 at Indira Gandhi Centre of Atomic Research, Kalpakkam, Tamilnadu, India.**

PREFACE

Physics based deformation models play a crucial role in the safe life estimation of creep exposed components and for providing insights about hot working processes. Examining the creep and flow response of the metals employing constitutive models pertaining microstructural-based input parameters and variables helps in understanding of deformation characteristics that in turn influence the response of the material during creep and metal forming operations. Modeling and simulation can be a proficient alternative technique that provides the solutions and insights about the various issues. Creep phenomena and metal hot working both involves the movements of dislocations. Therefore, the mechanisms of substructure evolution involve similar physics for both the cases. Since creep research focuses on limiting strain and strain rates at high temperatures, hot working studies aim to at relatively higher strain rates between 10^{-2} and $10^2/s$. In either creep or hot deformation, the dislocations are the mostly responsible for accommodating plastic deformation. Therefore, while capturing their interactions dislocation density-based models can be developed that provide the anatomy of the induced microstructure with ongoing creep as well as during hot working. In this direction, dislocation density based physical modeling is a decent choice, as it elucidates the complex deformation behaviours as well as provides the insights about the ongoing substructure evolution. The main objective of this research work done in this thesis is to develop microstructure-based creep and flow stress models to reveal the substructure evolution with ongoing deformation. In each of the chapter, an improved model is presented that fills the gap in the literature to some extent.

Chapter 01. Considering the physics-based approaches flow stress models [4, 5, 34, 37, 63] are represented as,

$$\sigma = f(\sigma_0, \rho, \lambda_{mean}) \quad (1.1)$$

where σ_0 refers to the contribution from short range barriers, ρ is the average dislocation density and λ_{mean} being the mean free path of the dislocations. Following issues were observed with respect to flow stress models.

- A physical based model which also incorporates annealing twin density effect and explains the microstructural evolution during plastic deformation of low stacking fault energy material was not found.
- Most of the flow stress models predicts the microstructure evolution along with flow stress response but the velocity of dislocations and influence on recrystallization phenomena was not observed.
- All the experimental curves are fitted with the models, limiting the prediction capabilities.
- Individual contribution of different type of strengthening was rarely addressed.

Similarly, creep rate is modelled as,

$$\dot{\epsilon} = f(\rho_m, \rho_b, \rho_{dip}, R_{sub}, T, \sigma_{appl}, N_v, r_p, D_{cav}, D_{ppt}), \quad (1.2)$$

where, ρ_m is mobile dislocation density, ρ_b is boundary dislocation density, ρ_{dip} is dipole dislocation density, R_{sub} is the subgrain radius, N_v is the number density of the precipitate, T is temperature, σ_{appl} is applied stress, D_{cav} is the cavitation damage and D_{ppt} is damage due to coarsening of precipitates.

The problem lies in a way that, if models address complete creep curve then microstructural evolution and all other important parameters are not demonstrated [14, 43, 66]. Impact of all

internal variables during the creep exposure is very important and rarely reported. Following issues were observed with existing creep models:

- Slip systems were not incorporated in rate equations of microstructural evolution.
- Influence of stacking fault energy on dislocation velocities was not considered.
- Complex dislocation climb velocity models were used.
- Temperature dependent shear modulus was not incorporated.
- Evolution of some variables was ignored in the literature, that are boundary dislocation spacing, subgrain boundary mobility, dipole capture spacing, climb stress, mean radius of precipitates
- Evolution of damage due to different types of precipitates was not demonstrated separately.
- Temperature and time dependent mobility model for subgrain boundary migration was not implemented.

In light of these issues, physics based flow stress and creep models were developed in the subsequent chapters to address these issues.

Chapter 02. As the flow stress is a crucial parameter in understanding thermomechanical processes such as extrusion, rolling, forging, and other manufacturing processes, its modelling depends on complex microstructures that enable the definition of internal variables. In order to get more insights about the microstructure evolutions during the hot deformation a physical-based model for DDRX that validates the simulation results in terms of flow curves, dislocation density, DDRX fraction, and the predicts the dislocation velocities is a need. In this chapter a flow stress model was developed and validated with the experimental data of IN 718WP.

The key points of this new model is given below,

$$\sigma_{deform} = \underbrace{\sigma_{dis} + \sigma_{HP}}_{\text{athermal stress}} + \underbrace{\sigma_{ss} + \sigma_{gen}}_{\text{thermal stress}} \quad (2.1)$$

In Equation (2.1), where σ_{dis} , σ_{HP} , and σ_{ss} are the strength contributions due to dislocations, grain size and solid solutions, respectively. σ_{gen} represents strength contribution due to interaction among orthogonal dislocations. The estimation of v_{gl} can be done using the following approach [107],

$$v_{gl} = \lambda_{mean} v_0 \exp\left(-\frac{\Delta G}{k_B T}\right) \text{sign}(\sigma_{SReff}) \quad (2.2)$$

In Equation (2.2), λ_{mean} is the mean free path can v_0 is attempt frequency, ΔG is the average activation energy needed to encounter the obstacles, k_B is the Boltzmann constant and σ_{SReff} is the difference between the total flow stress and athermal stress as orthogonal dislocations. The mean free path can be estimated by considering the Pythagorean summation and taking all the possibilities as [113],

$$\frac{C_k}{\lambda_{mean}} = \frac{1}{h_m} + \frac{1}{s} + \frac{1}{g_{avg}} \quad (2.3)$$

Herein, C_k is the dislocation interaction coefficient, s is dislocation substructure size, g_{avg} is the average grain size and h_m is mobile dislocation spacing. The total flow stress ($\sigma_{total,flow}$) response during the hot deformation is estimated using the rule of the mixture of non-recrystallized and recrystallized areas as [116],

$$\sigma_{total,flow} = (1 - X_{DDRX})\sigma_{deform} + X_{DDRX}\sigma_{DDRX} \quad (2.4)$$

Where X_{DDRX} is recrystallization fraction, σ_{DDRX} is the flow stress contribution from DDRX region and σ_{deform} is the flow stress response from unrecrystallized region. The dislocation density-reliant flow stress model was developed by considering the physics behind DDRX phenomena to address the complete flow stress curve as well as microstructure evolution for the

IN718WP superalloy. Model capabilities for microstructure prediction was validated by comparing the results obtained with EBSD data in terms of dislocation density and DDRX fraction.

The important conclusions of this work are,

- Model predicts the flow stress response with a single set of calibrated parameters for the wide range of temperature and strain rate.
- The average grain size was observed to be decreasing and approaching to steady state easily at low strain rates or higher temperatures as compared to that of higher strain rates or lower temperatures.

Chapter 03. In this chapter a flow stress model was developed that includes the addition of twin boundaries as a strengthening elements as a new addition to previous developed models [34]. The model was validated with respect to flow curves of IN718 [4]. Total flow stress response can be expressed as,

$$\sigma_{flow} = \sigma_{dis} + \sigma_{HP} + \sigma_{ss} , \quad (3.1)$$

Herein, the strengthening contribution from the dislocation is given by Taylor hardening relations,

$$\sigma_{dis} = \alpha M G_{sm} b \sqrt{\rho_i} , \quad (3.2)$$

Herein, α is a parameter that is dependent on the dislocation interactions, ρ_i is immobile dislocation density, M is the Taylor factor, b is magnitude of Burgers vector and G_{sm} is shear modulus. Furthermore, by incorporating the twin boundary concept [137], the grain boundary strengthening contribution is calculated using the modified Hall-Petch contribution and is represented as [34],

$$\sigma_{HP} = \frac{K_{HP} G_{sm}(T)}{\sqrt{g_{eff} G_{RT}}} = \frac{K_{HP} G_{sm}(T)}{\sqrt{g} G_{RT}} \left[1 + 2K_t \ln \left(\frac{g}{g_0} \right) \right]^{\frac{1}{2}} . \quad (3.3)$$

Herein K_{HP} is the Hall-Petch strengthening coefficient, $G_{sm}(T)$ is temperature dependent G_{sm} , G_{RT} is room temperature G_{sm} and K_t is a constant, g is the grain size before annealing and g_0 is the grain size after annealing. The short range contribution provided by the solid solutions is estimated through the following expression [138],

$$\sigma_{ss} = \left[\sum_{i=0}^n Z_L G(T)^{\frac{3}{2}} (\alpha_s \delta_i + \dot{\eta}(T))^2 c_i \right]^{\frac{2}{3}}, \quad (3.4)$$

Herein Z_L is a material parameter, c_i is solute concentration α_s is a dimensionless constant and $\dot{\eta}(T)$ is the temperature-dependent misfit of G_{sm} . The major outputs of the model are discussed below,

- The contributions of dislocation strengthening and Hall-Petch strengthening dominates over others with respect to the overall σ_{flow} .
- The predictions of flow responses are not good and there is significant deviation in experimental and predicted flow curves if twins are not considered and the traditional Hall-Petch equation is used.

Chapter 04. The anatomy of the induced microstructure with ongoing creep plays a crucial role in the safe life estimation of components and for the new alloys development programs. In this chapter a creep model was developed and validated with the experimental data of RAFM steel. The novelty of the model lies with [47, 57]:

- Implementation of temperature and time dependent mobility model for subgrain boundary migration as,

$$M_{sb} = \underbrace{\frac{2\pi\eta D_s \Omega}{bk_B T}}_{\text{Core mobility}} + \underbrace{\frac{2\pi b D_{vp} \Omega}{h_b^2 k_B T}}_{\text{Lattice diffusion mobility}} \quad (4.1)$$

Herein, η is the transfer coefficient of dislocation core to jogs and h_b is boundary dislocation spacing, D_{vp} is pipe diffusion coefficient and D_s is the lattice self-diffusion coefficient.

- A more simplified method is presented to evaluate the climb velocity and associated equations are presented in form of variables N_1 , N_2 and N_3 to obtain the climb stress and climb velocity.

Equation for the dislocation climb velocity can be given as,

$$v_{cl} = \frac{D_s \Omega \sigma_c}{bk_B T} \quad (4.2)$$

Combined equation for climb velocity and climb stress can be given as,

$$\sigma_{cl} + \frac{v_{cl}}{B_{vis}} = \frac{G_T b}{2\pi(1-\nu)} \frac{2}{d_{spon} + d_{dip}} \quad (4.3)$$

$$\sigma_{cl} - v_{cl} * N_1 = 0, \text{ where } N_1 = \frac{bk_B T}{D_s \Omega} \quad (4.4)$$

$$\sigma_{cl} + v_{cl} * N_2 = N_3, \text{ where } N_2 = \frac{1}{B_{vis}}, N_3 = \frac{G_T b}{2\pi(1-\nu)} \frac{2}{d_{spon} + d_{dip}} \quad (4.5)$$

$$\sigma_{cl} = \frac{N_3 * N_1}{(N_2 + N_1)} \quad (4.6)$$

- Temperature-dependent shear modulus is incorporated.
- Evolution of additional variables that were not discussed in the literature, those are boundary dislocation spacing, subgrain boundary mobility, dipole capture spacing, climb stress, mean radius of MX (V and Ta based carbonitrides) precipitates, mean radius of $M_{23}C_6$ carbides is presented and discussed thoroughly.
- Evolution of damage due to two different types of precipitates is demonstrated separately.

The following observation can be noted from the investigated conditions:

- Mobile and dipole dislocation density decrease with ongoing creep due to glide and climb recovery. In the beginning of creep exposure, boundary dislocation density is found to be increasing and afterward decreases due to dominance of subgrain growth.
- Radius of subgrain is found to coarsen with ongoing creep. The both dislocation velocities were found to be increasing with creep.
- The computed internal stress was observed to be decreasing with creep. The effective stress on dislocations was observed to be increasing with creep.

Chapter 05. Existing models LSFE materials either do not provide information about the microstructural changes occurring during creep or employ too many adjustable parameters. Thus, a sound model that considers the influence of SFE on dislocation velocities, explains the evolution of the internal variable along with creep curves, and works with a single set of calibration parameters is a need. In this chapter a creep model was developed and validated with the experimental data of IN718. The new equations that were implemented in this work are,

- Glide velocity:

$$v_{gl} = a_1 M \Gamma \left(\frac{1}{br_p} \right) v_{p,i} L_p C_j D_s \sinh \left(\frac{\sigma_{effe} b^2 L_p}{M k_B T} \right), \quad (5.1)$$

In Equation (5.1), $v_{p,i}$ is the phase fraction of the precipitates, a_1 is a prefactor for the gliding velocity, Γ is the stacking fault factor, X is the magnitude of the SFE, L_p is the mean spacing between all types of precipitates, σ_{effe} is effective stress and C_j is the jog density.

- Climb velocity

$$v_{cl} = \frac{\Omega D_{vp} \sigma_{cl}}{b K_B T} \cdot \Gamma, \quad (5.2)$$

- Rate equation of dislocation densities incorporated slip system information, for example,

$$\dot{\rho}_m = \underbrace{\left(\frac{\rho_m^+}{\lambda_{mean}} v_{gl} \rho_m \right)}_{\text{production}} - \underbrace{\left(\frac{v_{gl}}{s} \rho_m \right) \left(1 - \frac{1}{n_{slip}} \right)}_{\text{immoblization}} - \underbrace{d_{spon} \rho_m v_{gl} (\rho_m + \rho_i) \left(\frac{1}{n_{slip}} \right)}_{\text{glide recovery}}, \quad (5.3)$$

In Equation (5.3) ρ_i is immobile dislocation density, d_{spon} is the spontaneous annihilation distance, n_{slip} is the number of active glide systems and $s = k_c/(\rho_{imob})^{0.5}$ is the dislocation substructure size, where k_c is the calibration parameter. Herein, we assumed that the total number of active glide systems is n_{slip} , and an equal number of dislocations are available on each system. The normalisation will be $1/n_{slip}$, for any dislocation reaction. Furthermore, since the reaction partners are available on all glide systems, we replaced $1/n_{slip}$ with $(n_{slip}-1)/n_{slip}$ [113].

Experimental creep curves were modelled and validated up to the secondary stage. In addition to this, the model was shown to be capable of addressing the evolution of the internal variables such as ρ_m , ρ_i , λ_{mean} , v_{gl} , σ_{int} , σ_{effe} and σ_{cl} with creep time. To get more confidence about the model predictions, the boundary dislocation density estimated from the EBSD characterization was compared with the dislocation density predicted by the model. From the explored conditions following conclusions can be drawn,

- The model suggests that both the dislocation densities, internal stress and climb stress increase over the period of creep. Whereas the mean free path, glide velocity and effective stress have a decreasing trend.
- The proposed model is capable of addressing the effect of the stress and temperature on the primary to steady state creep regime using a single set of parameters.

Chapter 06. In this chapter a creep model was developed and validated with the experimental data of steel 316 LN.

This work presents some improvements compared to existing literature in the sense that,

- A more generalized mobility model is assimilated that considers temperature dependent maximum back stress.

$$M_{cg} = \frac{D_0 b}{k_B T} e^{\frac{\sigma_{eff} b^3}{k_B T}} e^{-\frac{Q}{RT} \left[1 - \left(\frac{\sigma_{eff}}{\sigma_{max}} \right)^2 \right]} \quad (6.1)$$

where, $\sigma_{max} = 1.5 \times \sigma_{UTS}$, and Q being the activation energy for self-diffusion.

In order to make the equation (6.1) more physical, temperature dependent ultimate tensile strength is incorporated to find the maximum back stress as $\sigma_{max} = 1.5 \times \sigma_{UTS(T)}$

$$\sigma_{UTS(T)} = -1.1241 T + 1411.8000 \quad (6.2)$$

- Effective stress was considered in place of applied stress for estimating dislocation glide velocity

$$v_{cl} = M_{cg} b \sigma_{eff} \quad (6.3)$$

- The temperature dependent shear modulus is incorporated

Outcome of this work is delineated in brief as,

- Mobile and forest dislocation density increase and average dislocation glide distance decreases with ongoing creep. The Internal stress is found to be increasing whereas the effective stress decreasing with ongoing creep.
- The velocity and mobility of dislocations decrease with accumulated strain. They were observed between 2.37×10^{-12} - 1.45×10^{-11} m/s and 1.61×10^{-10} - 3.41×10^{-10} mPa⁻¹s⁻¹, respectively.
- The damage caused by the carbonitrides precipitate (MX-type) and carbides precipitate (M₂₃C₆-type) are increasing with ongoing creep. Cavitation damage rate was found to be increasing with creep time.

References section provides the list of relevant references (258) cited in Chapter 1-6 of the thesis.